Supporting information for "Effect of donor content on the efficiency of P3HT:PCBM bilayers: optical and photocurrent spectral data analyses"

Mosé Casalegno,*[a] Dariusz Kotowski,[b] Andrea Bernardi,[c] Silvia Luzzati,[b] Riccardo Po,[c] and Guido Raos [a]

[a] Dipartimento di Chimica, Materiali e Ingegneria Chimica "G. Natta", Politecnico di Milano, Via L. Mancinelli 7, 20131 Milano, Italy.
[b]ISMAC, Via Edoardo Bassini 15, 20133 Milano, Italy.
[c]Research Center for Non-Conventional Energies, Istituto ENI Donegani, Eni S.p.A, Via G. Fauser 4, 28100 Novara, Italy.

Optical data

In this Section, we report the refractive indexes and the extinction coefficients obtained from VASE measurements, and used in all TMM calculations. As specified in the text, optical constants were determined for ITO, PEDOT:PSS, P3HT, and PCBM. ITO was deposited on glass, whereas the other materials on a Si substrate, in order to enhance the spectral response and remove backside reflections. Figure S1, shows the refractive indices and the extinction coefficients for all pristine materials, except P3HT (see the discussion below). Our estimates are comparable with those reported in the literature[1] for the same materials.

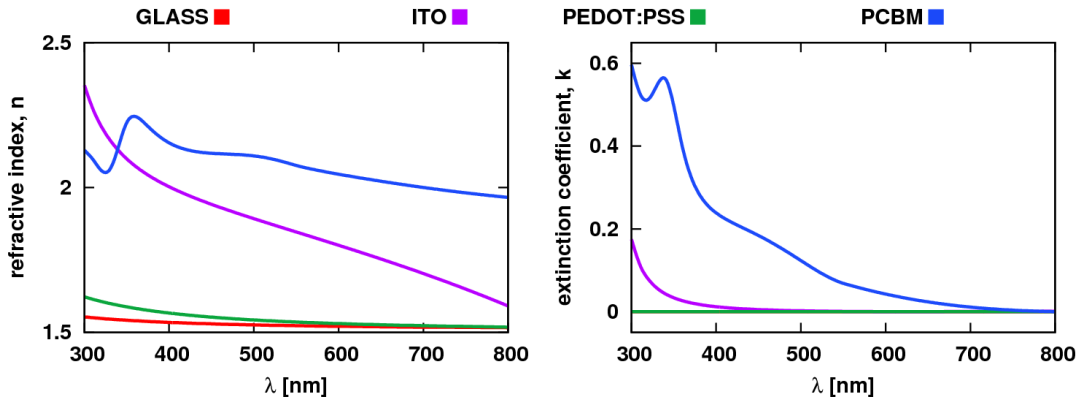

Fig. S 1: Measured refractive indices (left) and extinction coefficients (right) for OSC materials (except P3HT).

Preliminary calculations of optical absorption spectra with the TMM algorithm, revealed for P3HT a spectral behavior different than expected. In particular, we were not able to satisfactorily fit the experimental absorption spectra of our devices, regardless the PCBM volume fraction. Figure S2 provides an example of this outcome for device P2. The simulation setup is analogous to that used in Fig. 2. It is easy to note that all simulated spectra lack the peaks around 520, 550, and 600 nm. As mentioned in the text, these spectral features can be associated with the π-π^* transitions in ordered films of pristine, regioregular P3HT.

Further analysis of P3HT data confirmed that the deposition of P3HT on a Si substrate had a negative effect on the sample cristallinity, leading to an amorphous, rather than cristalline, film. To further support this conclusion, we measured the optical density of a thin P3HT film (50 nm), deposited on a glass:ITO:PEDOT substrate. Layer thicknesses were analogous to those used in device assembling. Figure S3 shows the measured optical density of the film. For comparison, we also reported two profiles resulting from TMM calculations carried out on the same film. The experimental optical density clearly shows the vibronic structure of crystalline P3HT. Use of P3HT optical constants determined by VASE on Si — violet curve — was not able to recover these spectral features. For this reason, literature data[1] — green curve — were preferred instead.

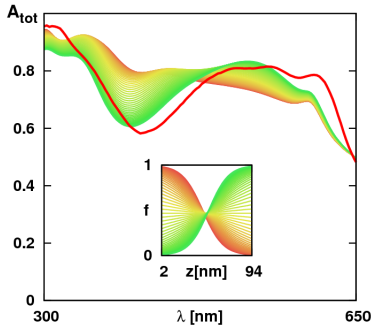

Fig. S 2: Experimental (red) and simulated total absorption spectra for device P2. The inset shows the corresponding PCBM volume fractions ($f(z)$).

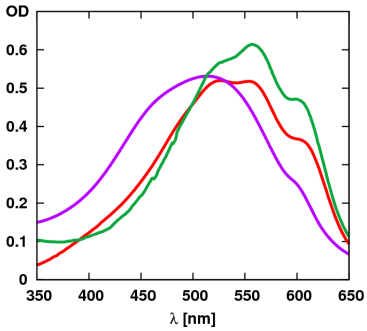

Fig. S 3: Experimental (red), and calculated optical densities for a 50-nm film deposited on glass:ITO:PEDOT substrate. Calculations were performed with the TMM algorithm. P3HT optical constants were either determined by VASE (violet), or taken from the literature[1] (green).

The PCBM volume fraction: calculation of the constrained parameters

Hereafter, we shall calculate the values of the parameters b and d in Eq.(2) (see text). The parameter b was chosen to ensure an appropriate behavior of $f(z)$ for $c = 0$, in which case the PCBM fraction reduced to a constant:

$$f(z, c = 0) = \frac{1}{1 + b} = \frac{L_{PCBM}}{L}\,, \tag{S-1}$$

where $L = L_{PCBM} + L_{P3HT}$. Solving with respect to b, gives:

$$b = \frac{L_{P3HT}}{L_{PCBM}}\,. \tag{S-2}$$

The parameter d was chosen to keep the overall amount of PCBM constant, and equal to L_{PCBM} (44 nm, in this case). This condition can be epressed mathematically as:

$$I = \int_{z_{inf}}^{z_{sup}} f(z)\, dz = L_{PCBM}\,, \tag{S-3}$$

where $z_{inf} = \ell/2$ nm, and $z_{sup} = L + \ell/2$, represents the lower and upper active layer boundaries, respectively. The above integral can be soled analytically to give:

$$I = z_{sup} - z_{inf} + ln\left[\frac{1 + b \cdot e^{c\,(z_{inf} - d)}}{1 + b \cdot e^{c\,(z_{sup} - d)}}\right]\,. \tag{S-4}$$

Combining S-3 with S-4, and solving for d, gives:

$$d = ln\left[\frac{b\,(g\, e^{c\, z_{inf}} - e^{c\, z_{sup}})}{1 - g}\right]\,. \tag{S-5}$$

where,

$$g = e^{(L_{PCBM} + z_{inf} - z_{sup})} \,. \tag{S-6}$$

EQE simulation setup and parameters

The calculation of EQE spectra was performed combining the TMM model with the 3DME method[2]. As stated in the text, only exciton dynamics was simulated explicitly. The geminate pair and charge dynamics were taken into account implicitly, as described in the text. EQE simulations were carried out using a wavelength-dependent light intensity drawn from the AM1.5G spectrum. At each wavelength, the exciton generation profile was obtained from the TMM algorithm. The photoactive layer was represented as a three-dimensional network of A and D sites. The algorithm used to generate model morphologies for these simulation is described in the next section. The master equations describing the dynamics of excitons were then solved iteratively on each site. The same parameters were used for A and D sites, indifferently. The rate constants for exciton hopping and decay were obtained from the exciton diffusion length and coefficient, as described in our previous works[2,3]. Table S1 collects the parameters used in all simulations. Each simulation was stopped after two thousand iterations. All simulations were excuted in parallel to cut down the CPU cost.

Table. S 1: Exciton dynamics parameters.

Parameter	Symbol	Value	Unit	Comment
Exciton hopping rate*	w^{exh}	$2 \cdot 10^{-2}$	ps^{-1}	ref.[4–9]
Exciton decay rate*	w^{exd}	$4 \cdot 10^{-3}$	ps^{-1}	ref.[4–9]
Exciton dissociation rate	w^{exs}	20.0	ps^{-1}	ref.[10]

Morphology: generation algorithm and optimization procedure

The generation of active layer morphologies, used for the calculation of EQE spectra, was performed using a simple algorithm developed by our group. All sites in the photo active layer were initialized as D sites. N sites, hereafter called seeds, were chosen at random in the first layer (e.g. $z = \ell$), and turned into A sites. To each i-th site within the first layer, a score was assigned according to the following equation:

$$s_i = \sum_{n=1}^{N_{XY}} \frac{1}{1 + r_{in}} \,, \tag{S-7}$$

where r_{in} represents the distance between the i-th site and the n-th seed. In order to account for periodic boundary conditions along the x and y axes, we considered the minimum image distance between each pair of sites:

$$r_{in} = min|\bar{r_n} - \bar{r_i}| \,, \tag{S-8}$$

where $\bar{r}_i$ represents the position of the i-th site, whereas, $\bar{r}_n$ the position of the n-th seed. Eq. (S-7) was used to rank the sites in decreasing order. Starting from the top rank sites, all D sites were turned into A sites, so to reach the D-to-A ratio specified by the PCBM volume fraction ($f(z)$). This allowed for the construction of P3HT:PCBM phase separated morphologies.

The same procedure was then applied to all layers ($z \leq L$, with $L = L_{P3HT} + L_{PCBM}$) without changing the position of the initial A seeds in the xy plane. At the end of this procedure, a random number was drawn for each layer. For the numbers exceeding a numerical threshold, R, all A sites were shift randomly in x and/or y direction, up to a maximum value, K. Periodic boundary conditions were also applied to all sites on crossing the simulation box boundaries. The algorithm above described was implemented within the 3DME code. Two additional layers of sites were placed at the bottom ($z = 0$) and the top ($z = L + \ell$) to represent the cathode and the anode, respectively.

Figure 4 shows the effect of the parameters N, K and R on the active layer morphology of device P3. In these examples, we assumed an uniform PCBM distribution across the active layer. Morphologies M_1 and M_2 are both characterized by one PCBM domain ($N = 1$). M_2, however, shows a larger D/A surface, due to higher values of K and R. This can be expected to improve exciton dissociation and therefore to increase the EQE. As shown in the last example, M_3, increasing N greatly enhances the D/A surface area, and was used in this work to further control the exciton dissociation efficiency, and the EQE intensity. In fact, as mentioned in the text, these parameters had no

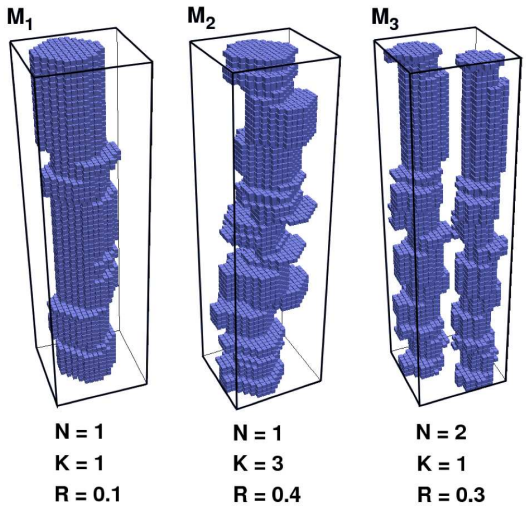

Fig. S 4: An example of three model morphologies obtained for device P3, assuming an uniform PCBM distribution across the active layer. For clarity only PCBM sites are shown.

significant effect on the EQE spectral behavior.
For a given PCBM volume fraction, the parameters N, K, and R were manually varied in order to match the experimental EQE intensity. The root-mean-square deviation was used as goodness-of-fit function and calculated in the range between $\lambda = 350$ nm and $\lambda = 600$ nm. Table S2 summarizes the values of N, K, and R obtained for the two sets of c values considered in this work: S_A and S_{EQE} (see text). For device P4, increasing the number of PCBM seeds beyond 10 did not increased the EQE intensity, nor it improved the agreement with the experimental data.

Table. S 2: Values of N, K, and R for S_A and S_{EQE}.

Device	S_A:	N	K	R	S_{EQE}:	N	K	R
P1		3	1	0.4		3	2	0.3
P2		3	2	0.4		3	2	0.4
P3		3	1	0.1		3	2	0.8
P4		3	1	0.05		10	2	0.5
P5		3	2	0.6		2	2	0.3
B6		3	1	0.5		3	1	0.5

References

[1] G. F. Burkhard, E. T. Hoke and M. D. McGehee, *Adv. Mater.*, 2010, **22**, 3293–3297.

[2] M. Casalegno, A. Bernardi and G. Raos, *J. Chem. Phys.*, 2013, **139**, 024706.

[3] M. Casalegno, G. Raos and R. Po, *J. Chem. Phys.*, 2010, **132**, 094705.

[4] S. Cook, A. Furube, R. Katoh and L. Han, *Chem. Phys. Lett.*, 2009, **478**, 33–36.

[5] O. V. Mikhnenko, H. Azimi, M. Scharber, M. Morana, P. W. M. Blom and M. A. Loi, *Energy Environ. Sci.*, 2012, **5**, 6960–6965.

[6] P. E. Shaw, A. Ruseckas and I. D. W. Samuel, *Adv. Mater.*, 2008, **20**, 3516–3520.

[7] H. Wang, H.-Y. Wang, B.-R. Gao, L. Wang, Z.-Y. Yang, X.-B. Du, Q.-D. Chen, J.-F. Song and H.-B. Sun, *Nanoscale*, 2011, **3**, 2280–2285.

[8] J. E. Kroeze, T. J. Savenije, M. J. W. Vermeulen and J. M. Warman, *J. Phys. Chem. B*, 2003, **107**, 7696–7705.

[9] L. Lüer, H.-J. Egelhaaf, D. Oelkrug, G. Cerullo, G. Lanzani, B.-H. Huisman and D. de Leeuw, *Org. Electron.*, 2004, **5**, 83–89.

[10] S. Günes, H. Neugebauer and N. S. Sariciftci, *Chem. Rev.*, 2007, **107**, 1324–1338.